scientific reports

Check for updates

OPEN

Rapid photonic curing effects of xenon flash lamp on ITO–Ag–ITO multilayer electrodes for high throughput transparent electronics

Zhenqian Zhao[1], Alex Rose[3], Sang Jik Kwon[1], Yongmin Jeon[2]✉ & Eou-Sik Cho[1]✉

High-throughput transparent and flexible electronics are essential technologies for next-generation displays, semiconductors, and wearable bio-medical applications. However, to manufacture a high-quality transparent and flexible electrode, conventional annealing processes generally require 5 min or more at a high temperature condition of 300 °C or higher. This high thermal budget condition is not only difficult to apply to general polymer-based flexible substrates, but also results in low-throughput. Here, we report a high-quality transparent electrode produced with an extremely low thermal budget using Xe-flash lamp rapid photonic curing. Photonic curing is an extremely short time (~ µs) process, making it possible to induce an annealing effect of over 800 °C. The photonic curing effect was optimized by selecting the appropriate power density, the irradiation energy of the Xe-flash lamp, and Ag layer thickness. Rapid photonic curing produced an ITO–Ag–ITO electrode with a low sheet resistance of 6.5 ohm/sq, with a high luminous transmittance of 92.34%. The low thermal budget characteristics of the rapid photonic curing technology make it suitable for high-quality transparent electronics and high-throughput processes such as roll-to-roll.

As demand for electronics that can be attached, worn or implanted on the human body has grown, numerous studies have investigated various form-factors of flexible electronics, and transparent electronics for various applications[1–5]. Transparent and flexible electronics technologies are considered key elements for next generation displays, secondary batteries, solar cells, semiconductors, and healthcare devices[6–9].

Among the various fundamental technologies needed to achieve transparent and flexible electronics, transparent and flexible electrodes are particularly important. Research on transparent flexible electrodes is being conducted using various materials and processes, including transparent conductive oxides (TCO), 2D materials (MXene, Graphene), conductive polymers, and silver nanowires, with the goal of achieving high transmittance and high conductivity at the same time[10,11]. However, most of these transparent flexible electrode candidates have had difficulty achieving both high transmittance and high conductivity at the same time, due to process complexity, and optoelectrical trade-offs.

Among various electrodes, indium tin oxide (ITO) is the most commonly used transparent electrode because it has excellent characteristics, including both high transmittance and low resistivity (6.68×10^{-4} Ω cm)[12–14]. ITO is also used as an anode for various organic electronics including organic light-emitting diodes and polymer solar cells because of its high workfunction characteristics[15,16]. However, because the conductivity of TCOs is typically lower than that of metal-based electrodes, it's often necessary to lower ITO resistivity to improve the efficiency and power consumption of TCO-based electronic devices. In addition, an ITO electrode also has lower flexibility than a metal-based electrode. This has led to growing interest in the oxide-metal-oxide (OMO) structure, which has both mechanical flexibility and high conductivity. The metal thickness determines the transmittance and contributes to the conductivity of the OMO structure[17–19]. ITO–Ag–ITO multilayer electrodes are widely used because it offers better optical and electrical characteristics than ITO alone[15]. In the OMO structure, the choice of oxide materials is very wide, and can depend on the application[20–26]. However, ITO is a representative oxide candidate that satisfies all conditions, including high work-function, high transmittance and high conductivity, so that it can be used as an anode in organic electronics (organic light-emitting diode, polymer solar cell etc.), which are commonly used in flexible and transparent electronics[15].

[1]Department of Electronics Engineering, Gachon University, Seongnam 13120, Republic of Korea. [2]Department of Biomedical Engineering, Gachon University, Seongnam 13120, Republic of Korea. [3]PulseForge Corporation, Seoul 04070, Republic of Korea. ✉email: yongmin@gachon.ac.kr; es.cho@gachon.ac.kr

To achieve flexibility, the OMO electrode must be fabricated using a low-temperature process (< 150 °C), so that the flexible polymer substrate is not damaged. However, at low-temperature the non-stoichiometric ratio of deposited ITO films is not balanced[27,28], and the interface effect between layers will restrict its characteristics. As a result, the ITO–Ag–ITO multilayer must be annealed to improve its characteristics. The crystallinity of amorphous phase ITO–Ag–ITO can be improved by the annealing process. However, commonly used methods such as rapid thermal annealing are difficult to apply in high-throughput processes, because the high thermal budget process exposes the polymer to high temperature (over 300 °C) for a long time (more than 5 min)[29–35].

This long post-annealing process limits throughput, because it is difficult to use with a roll-to-roll (R2R) process, which is one of the advantages of transparent flexible electronics. Also, the poor thermal stability of Ag film makes it unsuitable for traditional annealing processes[36]. To realize a superior transparent flexible ITO–Ag–ITO electrode with high transmittance and high conductivity, while ensuring high-throughput, a post-annealing process with a low thermal budget is required to provide high transmittance and high conductivity, while ensuring high-throughput. Digital thermal processing using Xenon flash lamp annealing (Xe-FLA) is an ideal curing method that can be applied to heat-sensitive substrates while retaining the effects of previous heat treatments on thin films[37–40]. Many previous reports have examined the digital thermal processing effects on ITO and amorphous silicon thin films during Xe-FLA irradiation[37].

In this study, we report a high-throughput, high-performance transparent electrode with high transmittance and high conductivity, fabricated with an extremely low thermal budget through rapid photonic curing, based on Xe-flash lamp annealing (Xe-FLA). The Xe-FLA conditions were optimized by simulations, to ensure it could provide a sufficiently high photonic curing effect even in an extremely short time, on the μs-scale, at a high temperature of 800 °C or higher. By optimizing the Xe-FLA irradiation time, radiant power, energy density, and the thickness of the ITO–Ag–ITO electrode, the figure of merit (FOM), which indicates the transmittance and conductivity characteristics, was improved by up to 58%. Using this photonic curing effect, an ITO–Ag–ITO transparent electrode with a high transmittance of 92.34% and a low sheet resistance of 6.5 ohm/sq was demonstrated.

Results and discussion

Rapid photonic curing simulation and ITO–Ag–ITO electrode design. To fabricate flexible and transparent electronics using a high throughput roll-to-roll process, it is essential to have a low thermal budget annealing process at a low temperature and a short annealing time, to avoid damage to the polymer-based flexible substrate. Xe-FLA is a high efficiency process which allows short photonic curing in the us time scale, and can anneal the material at a low thermal budget, without damaging the flexible substrate[41–43]. Xe-FLA is one of the thermal annealing methods that can heat thin films in a very short time without damaging the substrate. Various studies have been reported on Xe-FLA based on the heat treatment effect[38–40,44].

Using rapid photonic curing with Xe-FLA, high-quality transparent flexible ITO–Ag–ITO electrodes can be fabricated with high throughput, as shown in Fig. 1a. The transparent electrode undergoes an electron transition after receiving the radiant energy, which in turn releases part of the heat energy from the high energy level to the low energy level, intensifying atomic vibration, causing the material to undergo a phase transformation[45,46]. A rapid photonic curing effect is induced by this mechanism, resulting in simultaneous high transmittance and high conductivity in the ITO–Ag–ITO multilayer. (Fig. 1b).

In this experiment, we used PulseForge 1300 equipment (*PulseForge Corporation*), which uses a xenon light source, and has a full range output spectrum (200–1500 nm), with high radiant energy density (maximum: 45 J/cm^2) and radiant power density (maximum: 35 kW/cm^2), which can address a diversity of experimental conditions[44,47]. The Xe-FLA based photonic curing condition is described in more detail in the "Materials and methods" Section.

Before the radiant photonic curing effect of the Xe-FLA was applied, ITO–Ag–ITO electrodes were designed and optimized to have high transmittance and conductance. The thickness of the ITO electrode was fixed at 48 nm, based on the number of sputter scans 0, 1, 2 and 3, and the Ag thickness was approximately 0, 6, 12 and 18 nm, respectively. Since Ag has higher conductivity than ITO, as the thickness of the Ag electrode increased, the ITO–Ag–ITO sheet resistance improved, but the transmittance showed a trade-off characteristic (Fig. 1c, d). When the Ag thickness was 0, 6, 12 and 18 nm, the sheet resistance of the multilayer was 58.53, 26.16, 9.35 and 5.24 ohm/sq, and the average transmittance was 86.2, 82.2, 82.4 and 73.3%, respectively (Fig. S1).

However, adding Ag can improve transmittance in some wavelength ranges. When the Ag thickness was 12 nm, the transmittance was obviously higher in the 557–787 nm range, and the maximum transmittance value was 94.5%. As a result, the transmittance of ITO–Ag–ITO can be influenced by the morphology of the Ag film[31]. Transmittance is also affected by the large amount of valence electrons on the metal surface, since surface plasmon elements will form when the light is incident. This will result in the formation of an electric field stronger than the excited electric field[48]. As a result, the transmittance at 550 nm, the wavelength with the greatest luminance to the human eye, reached a high of 92.4% when the thickness of the Ag was 12 nm (Fig. 1e).

FOM is the ratio of the average transmittance of visible light to sheet resistance, which is equivalent to $\mathrm{FOM} = \frac{T_a^{10}}{R_s}$ (T_a: average transmittance, R_s: Sheet resistance). Accordingly, a larger FOM value indicates that the opto-electrical characteristics of the ITO–Ag–ITO are relatively better. The FOM of a multilayer with Ag thickness increases is 7.99, 16.29, 48.74 and 42.29 [$\times 10^{-3}\ \Omega^{-1}$], respectively (Fig. 1f). It was confirmed that the FOM value of the OMO electrode with the Ag layer was higher than that without an Ag layer. The largest FOM was observed when the Ag layer was 12 nm. These results confirmed that the OMO structure is better than that of an ITO layer. Obviously, when the thickness of the Ag layer is 12 nm, there is a better trade-off between the transmittance and sheet resistance characteristics of the multilayer.

Before rapid photonic curing is applied, the temperature change in the Ag in the multilayer was analyzed considering the absorption of radiant energy, for various Ag layer thicknesses (Fig. 2a). The energy transmission

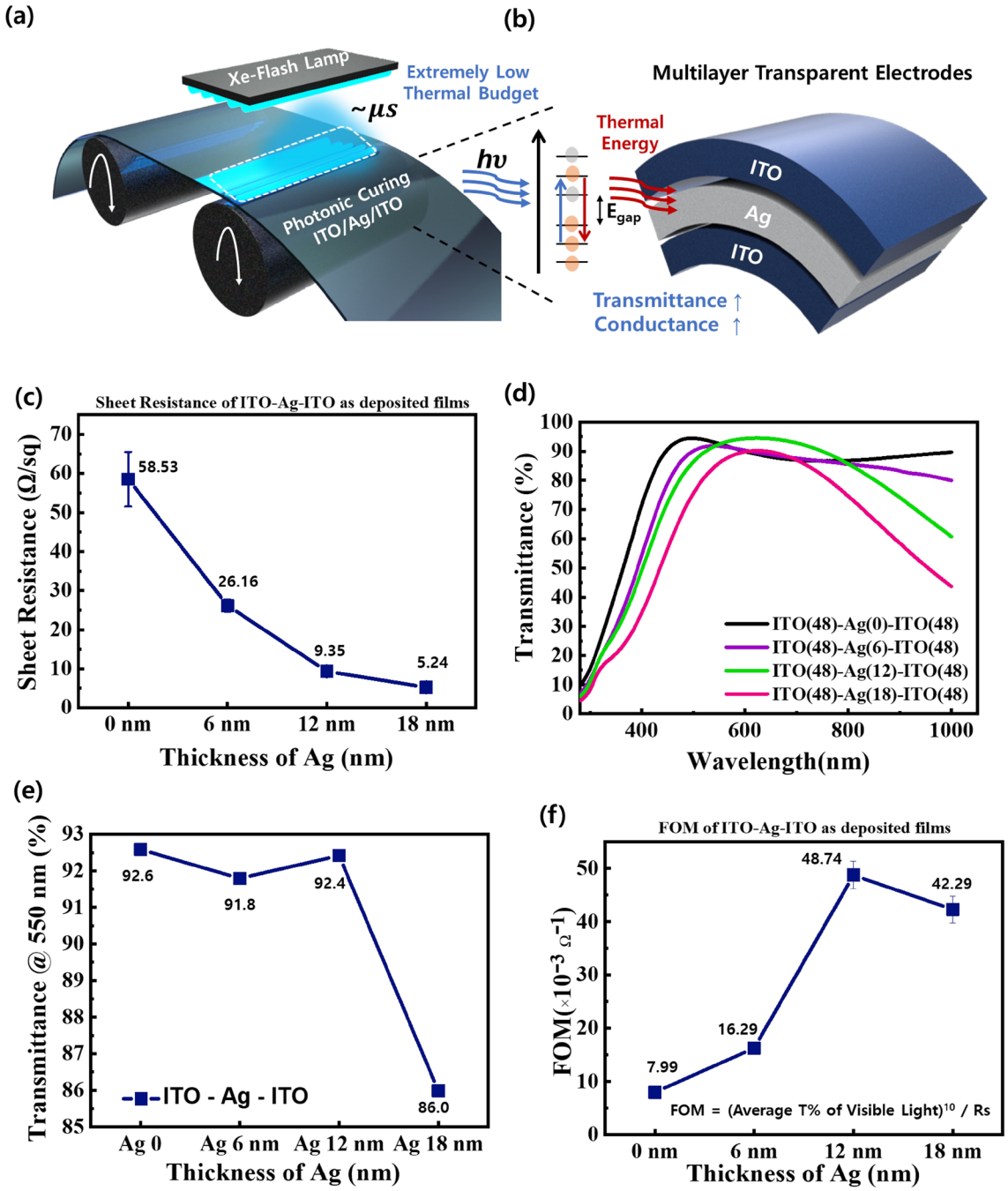

Figure 1. Concept of Rapid Photonic Curing using Xe-FLA and the Electro-optical Design of the ITO–Ag–ITO: (**a**) Schematic illustration of the R2R photonic curing of ITO–Ag–ITO (**b**) Schematic illustration of the ITO–Ag–ITO Xe-FLA mechanism. (**c**) Sheet resistance according to the Ag layer thickness in the multilayer electrode. (**d**) Transmittance according to Ag thickness in the ITO–Ag–ITO electrode. (**e**) Transmittance at 550 nm according to Ag thickness in the multilayer electrode. (**f**) FOM value according to Ag thickness in the multilayer electrode.

was measured using the bolometer of the PulseForge 1300 device. As shown in Fig. 2b, as the Ag thickness increased, the transmitted energy density decreased, and the energy absorptivity increased. These results suggest that the thicker the Ag layer becomes, the higher the heat temperature that will be transferred to the multilayer.

As shown in Fig. 2c and d, the ITO–Ag–ITO electrode peak temperature changes after absorbing radiant energy, as analyzed by SimPulse (PulseForge Corporation) software simulation. The simulation results in Fig. 2c show that an annealing effect of several hundred degrees Celsius can be applied to the film during microsecond scale rapid photonic curing. It was observed that the peak temperature increased as the thickness of the Ag, the radiant energy density, the radiant power density and the repeat times increased (Fig. 2c).

The highest peak temperature of 867 °C was observed when the radiant energy of 2.7 J/cm^2 was applied to the multilayer containing a 18 nm Ag layer (Fig. 2d). This high temperature was sufficient to anneal the ITO

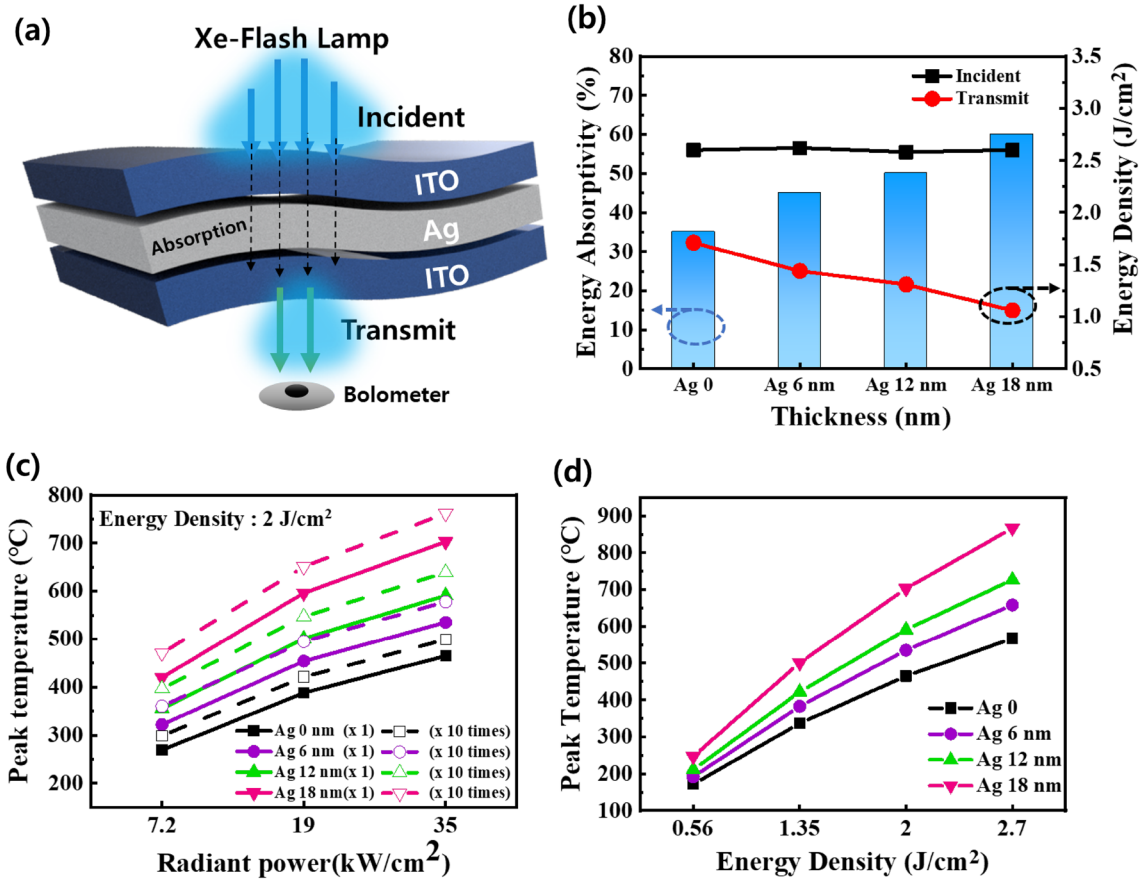

Figure 2. Analysis of Rapid Photonic Curing Annealing Temperature according to the Xe-FLA conditions: (**a**) Schematic illustration of the measured energy of Xe-FLA delivered to the ITO–Ag–ITO electrode. (**b**) Radiant energy absorptivity of different Ag thicknesses in the ITO–Ag–ITO electrode (@ 2.7 J/cm^2, 37 kW/cm^2, 100 μs). (**c**) Peak temperature at different Ag thicknesses, number of Xe-FLA irradiations, and radiant powers (@ 2.0 J/cm^2). (**d**) Peak temperature for different Ag thicknesses and radiant energy density of the ITO–Ag–ITO electrode.

single-layer, ensure it crystallized[49], and induce the Ag phase change[50]. Therefore, Xe-FLA has been applied to ITO and amorphous silicon thin films through the digital heat treatment effect on thin films. In addition, for Ag thin film, when thermal annealing is applied, electrical characteristics can be improved by the subsequent diffusion of Ag[32]. This simulation analysis confirmed which conditions were needed to achieve the annealing effect at a sufficient temperature when applying μs-scale rapid photocuring. Since high-temperature annealing occurs in a very short time period during photonic curing, very little thermal energy is transferred to the substrate, minimizing damage[41].

Analysis of electrical properties in relation to Xe-FLA conditions. Using the conditions determined by the annealing temperature analysis simulation, Xe-FLA-based photonic curing was applied to the ITO–Ag–ITO. Xe-FLA was applied with a radiant energy of 2 J/cm^2. The rate of change in ITO–Ag–ITO sheet resistance with different Ag thicknesses and radiant power is shown in Fig. 3a and Table S1. The sheet resistance of the OMO structure is composed of the parallel combination of sheet resistance of the ITO and that of Ag. Improving the electrical conductance of the ITO top and bottom oxide layers (Ag thickness of 0 nm) is a crucial factor for improving OMO performance.

As can be seen from the simulation results in Fig. 2, the higher the of Xe-FLA radiation power, the higher the peak temperature of the Ag thin film. As shown in this trend, in Fig. 3a, the sheet resistance improved as the annealing effect increased under the high peak temperature conditions after photonic curing. In addition, in the simulation results, it was confirmed that when Xe-FLA was applied 10 times under each radiant power condition, the reduction in sheet resistance also increased, like the tendency with temperature (Figs. S2, S3). The thinner the Ag layer, the greater the sheet resistance improvement effect, and the effect was maximized at a maximum radiation output of 35 kW/cm^2.

Figure 3b and Table S2 shows how photonic curing improved sheet resistance based on the thickness of Ag and the radiant energy of Xe-FLA at a radiant power of 35 kW/cm^2, where the photonic curing effect was the best. The simulation result in Fig. 2d confirms that the peak temperature increased in proportion to the thickness of the Ag and the energy density of the Xe-FLA at a radiant power of 35 kW/cm^2. The improvement in sheet resistance showed almost the same tendency (Fig. 3b). However, at an Ag thickness of 18 nm, when 2.7 J/cm^2 (~ 867 °C) of

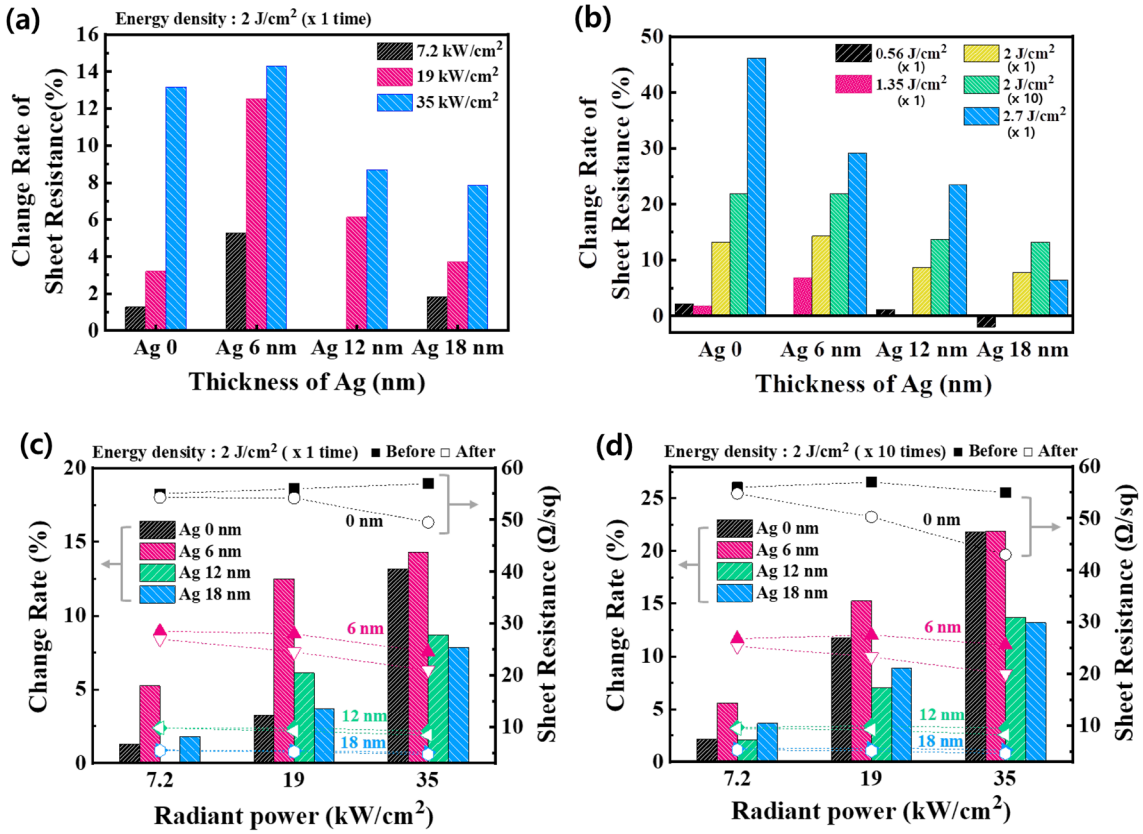

Figure 3. Electrical Properties Analysis according to the Conditions of Xe-FLA: (**a**) Change in sheet resistance for different Ag thicknesses and radiant powers (@ 2 J/cm^2, × 1 time) (**b**) Change in sheet resistance for different Ag thicknesses and radiant energy densities (0.56 J/cm2–24 kW/cm2, others–35 kW/cm^2). (**c**) Change in sheet resistance for different Ag thicknesses and radiant powers (@ 2 J/cm^2, × 1 time). (**d**) Change in sheet resistance for different Ag thicknesses and radiant powers (@ 2 J/cm^2, × 10times).

Xe-FLA was applied once, the improvement in sheet resistance was lower than when 2 J/cm^2 was applied 10 times (~ 762 °C). This result confirms that the photonic curing effect was decreased at a temperature of about 800 °C or higher. In the general thermal annealing method, if the Ag layer is annealed for a long time at a temperature of 300 °C or higher, there is a possibility that the sheet resistance will increase due to aggregation[30]. However, with the photonic curing method in this study, heat was transferred to the electrode for a very short time, in units of μs, and the sheet resistance was improved at a relatively high temperature of about 800 °C.

Figure 3c, d, and Table 1 show the sheet resistance and rate of change according to the radiant power of the Xe-FLA, at a radiant energy of 2 J/cm^2, which resulted in improvement under all conditions. When the Xe-FLA was irradiated 10 times at a radiant energy of 2 J/cm^2, the improvement in sheet resistance of the multilayer electrode was the highest, at 21.9% (25.6 → 20.0 ohm/sq) when the Ag thickness was 6 nm. Also, when the Ag thickness was 12 and 18 nm, respectively, similar sheet resistance improvements of 13.7 and 13.2% were observed.

Energy density (Repeat)	Ag (nm)	Sheet resistance		
		Before Xe-FLA (ohm/sq)	After Xe-FLA (ohm/sq)	Enhancement (%)
2 J/cm^2 (× 1 time)	0	57.0	49.5	13.2
	6	24.5	21.0	14.3
	12	9.2	8.4	8.7
	18	5.1	4.7	7.8
2 J/cm^2 (× 10 times)	0	55.0	43.0	21.8
	6	25.6	20.0	21.9
	12	9.5	8.2	13.7
	18	5.3	4.6	13.2

Table 1. Improvement in Sheet Resistance after Applying Xe-FLA Photonic Curing.

At an Xe-FLA radiant power of 35 kW/cm^2, which resulted in the best improvement, the improvement in sheet resistance was much greater with a 6 nm layer of Ag, compared to the effect at 12 or 18 nm of Ag. The reason for this is that at Ag 6 nm, Ag is not a continuous film but forms an island-like morphology, and thus has a relatively low sheet resistance. Although it depends on the process conditions, it is generally known that to form a continuous quasi-perfect layer the Ag thickness should be 9 nm or more[51]. Ag thicknesses of 12 and 18 nm produced a quasi-perfect layer, which already had a low sheet resistance before Xe-FLA application, so a relatively low improvement rate was obtained.

To achieve an OMO structure transparent flexible electrode with high transmittance, it is important to form a continuous film while reducing the Ag thickness as much as possible. However, since Ag thin film is generally formed by the Volmer-Weber 3D-island growth model, when Ag is deposited with a thickness of less than 9 nm, a quasi-perfect continuous film cannot be formed, and instead it has a relatively island-like morphology. When Ag is deposited at a thickness of 10 nm or more, a quasi-perfect layer that connects the Ag islands is formed, and the sheet resistance is greatly reduced. However, a thicker Ag layer has a trade-off relationship with decreasing transmittance. Various studies have reported methods of forming a continuous film even with a thin Ag layer, such as inserting a seed layer with high surface energy[52].

In the ITO–Ag–ITO multilayer in this study, 6 nm Ag formed as an island shape, and Ag 12 and 18 nm formed as a quasi-perfect layer (Fig. 4a). According to the SEM results, the surface morphology of ITO-Ag was exactly consistent with that of ITO–Ag–ITO[53]. Therefore, the trends in Ag morphology can be observed using SEM of the ITO–Ag–ITO surface. The sheet resistance significantly decreased at the boundary between Ag thicknesses of 6 and 12 nm (Fig. 3, Table1). Thin Ag grows island-like structures because the surface energy of the substrate is low. It was reported that the morphology and conductivity of an Ag layer sandwiched between ITO were improved due to the diffusion of Ag atoms even after treatment at a high temperature of over 500 °C[32]. In this study, the Xe-FLA diffused the Ag atoms at the same time as the phase change of the Ag, as shown in Fig. 4b, so that a more continuous film was formed.

The SEM image in Fig. 4c confirms that quasi-perfect morphology layers, like those for Ag 12 and 18 nm, were formed even at Ag 6 nm after Xe-FLA was applied (Fig. 4d, e). The SEM image results (Fig. 4c) also show that as the Xe-FLA radiant power increased, a more continuous film was formed, following the trend in sheet resistance reduction. For 12 and 18 nm Ag, although a quasi-perfect layer was initially formed, after the application of Xe-FLA the sheet resistance declined due to the formation of a more perfect film. As the radiant power was increased, SEM images confirmed that the Ag film morphology was more continuous (Fig. 4d, e).

Analysis of optoelectrical properties according to Xe-FLA conditions. The improvement in the optical properties of the OMO by Xe-FLA photonic curing was analyzed through average transmittance, and the improvement in optoelectrical properties was analyzed using the FOM value. The morphological tendency in the ITO–Ag–ITO after applying Xe-FLA was confirmed by analyzing SEM images. The transmittance of ITO–Ag–ITO is very closely related to the change in Ag morphology. A previously reported, the ITO/Ag/ITO transmittance gradually decreases when Ag is an island-structure, but gradually improves when the Ag forms a quasi-perfect layer.

First, as shown in Fig. 5a, when 2 J/cm^2 of radiant energy was applied to 6 nm Ag, as the radiant power increased, the average transmittance proportionally improved. This effect followed the same tendency as the previously observed improved resistance. However, for the 12 nm thick Ag, the improvement in transmittance at 19 kW/cm^2 radiant power was greater than that of 35 kw/cm^2, and in the case of 18 nm thick Ag, the transmittance decreased under all radiant conditions. When 2 J/cm^2 of Xe-FLA was applied 10 times, the transmittance also showed additional improvement depending on the conditions, but it was not as significant as the improvement in sheet resistance (Fig. S4).

The transmittance characteristics of the ITO–Ag–ITO were analyzed at different radiant energies, and number of irradiations, at an Xe-FLA radiant power of 35 kw/cm^2 (Fig. 5b). When the Ag thickness was 6 nm, the transmittance improved up to a radiant energy of 2 J/cm^2, but the transmittance significantly decreased at 2.7 J/cm^2. As shown in Fig. S5, under the energy condition of 2.7 J/cm^2, the transmittance shape of the full spectrum was deformed under all OMO electrode conditions, including the Ag. It can be seen that distortion of the Ag morphology was induced due to the high temperature of the applied 2.7 J/cm^2 energy. At 2 J/cm^2, 35 kW/cm^2 and 10 repeats, the average transmittance increased from 82.1 to 87.3%. On the other hand, for Ag thicknesses of 12 and 18 nm, transmittance decreased under most radiant energy conditions, and improvement in transmittance was only seen under some specific conditions (Ag 12 nm: 2 J/cm^2 irradiation once, Ag 18 nm: 2 J/cm^2 irradiation 10 times).

As described above, due to the Xe-FLA photonic curing, at Ag 6 nm, the island-like thin film was rough, and the transmittance improved as a quasi-perfect layer was formed. Therefore, when the Ag was 6 nm, the transmittance improvement also increased according to the power and the number of irradiations at a radiant energy of 2 J/cm^2 (Fig. S6). On the other hand, since the 12 nm and 18 nm Ag formed a quasi-perfect layer from the beginning, the Xe-FLA did not significantly improve transmittance, but when the roughness was improved depending on the conditions of irradiation, improved transmittance was observed (Fig. S6).

The value of FOM for both the conductivity and transmittance of the transparent electrode is important. Figure 5c and Table 2 show the FOM improvement ratio and values according to radiant power when Xe-FLA photonic curing of 2 J/cm^2 was applied. The 6 nm-thick Ag, which had the greatest electro-optical improvement after photonic curing with Xe-FLA, showed the greatest FOM improvement, and the 12 nm-thick Ag showed the second highest FOM improvement. However, 18 nm thick Ag showed a somewhat decreased FOM due to the decrease in transmittance, despite the improved conductance. When the radiant energy of 2 J/cm^2 was applied

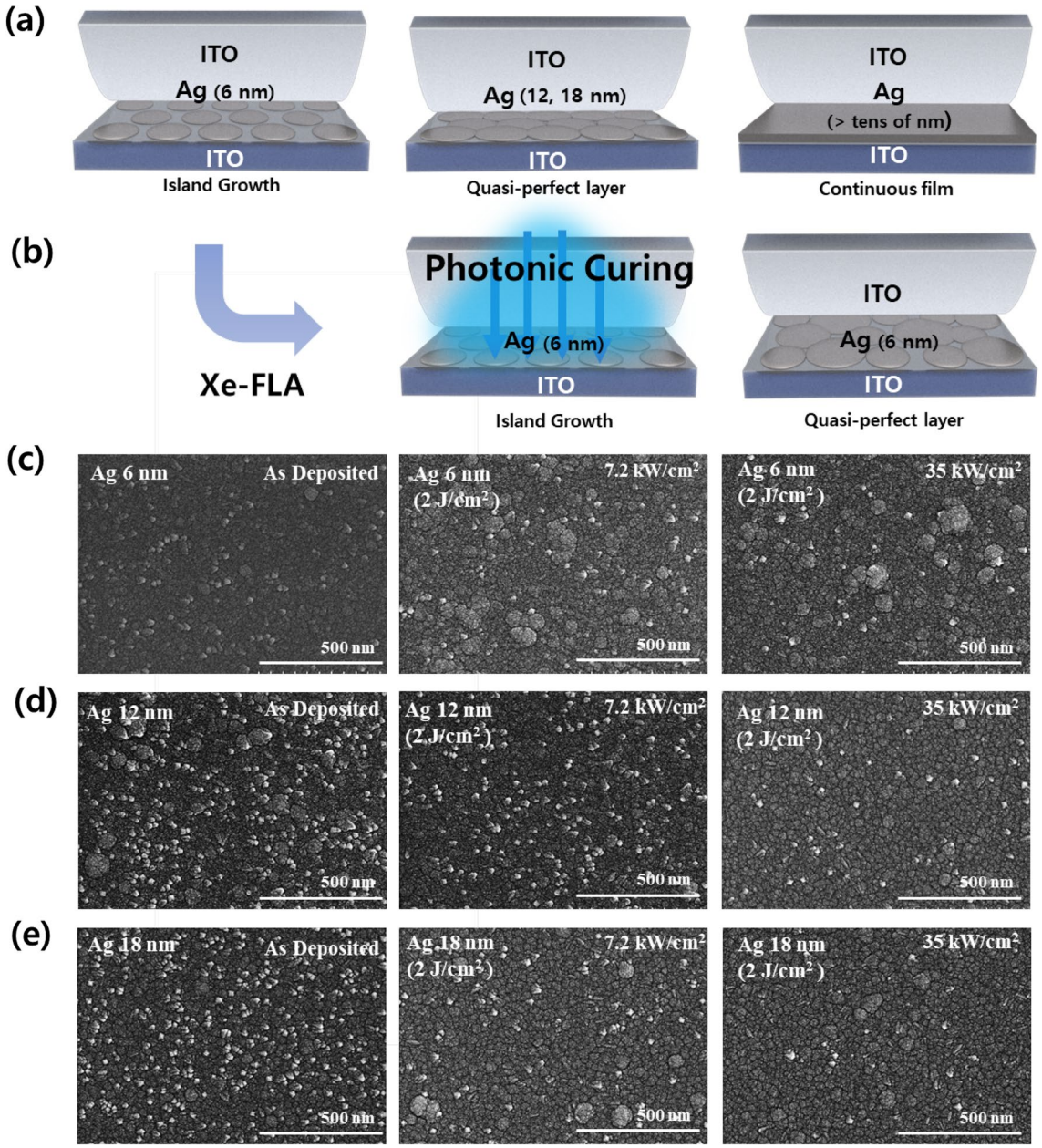

Figure 4. SEM Image of ITO–Ag–ITO Surface Morphology according to Photonic Curing of Xe-FLA: (**a**) Surface morphology for different thicknesses of Ag deposited via the Volmer-Weber 3D-island growth model. (**b**) Quasi-perfect Ag layer formation due to photonic curing effect using Xe-FLA. (**c**) SEM image of different Xe-FLA radiant powers for Ag 6 nm. (**d**) SEM image of different Xe-FLA radiant powers for Ag 12 nm. (**e**) SEM image at different Xe-FLA radiant powers for Ag 18 nm.

10 times, the FOM improvement differed depending on the conditions, and in particular, the 6 nm Ag showed a maximum FOM value improvement of 58% under a radiant power of 35 kW/cm^2 (Fig. S7, Table 2).

The effect of photonic curing at a radiant energy at 35 kW/cm^2, which had the best FOM improvement, is shown in Fig. 5d. At a Ag thickness of 6 nm, the FOM improvement was proportional to the energy of 2 J/cm^2. However, at an energy of 2.7 J/cm^2, the FOM value decreased because the transmittance decreased after Xe-FLA. Because of the excellent basic electrical characteristics of the multilayer with an Ag layer thickness of 12 nm, the maximum value of FOM was 69.33 under photonic curing conditions of 2.7 J/cm^2 with a radiant power of 35 kW/cm^2.

To confirm the effect of Xe-FLA on the surface of the multilayer, an atomic force microscope (AFM) was used to observe the multilayer morphology. The multilayer with an Ag thickness of 12 nm, which had the maximum FOM value, was selected for AFM observation (Fig. 6). The AFM image confirmed that the surface roughness was improved after photonic curing at 2 J/cm^2 compared to before Xe-FLA annealing. The photonic curing results confirmed that the conditions for improving transmittance and the conditions for improving surface roughness were the same (Figs. 5b, 6). However, after photonic curing at 2.7 J/cm^2, the transmittance showed similar or

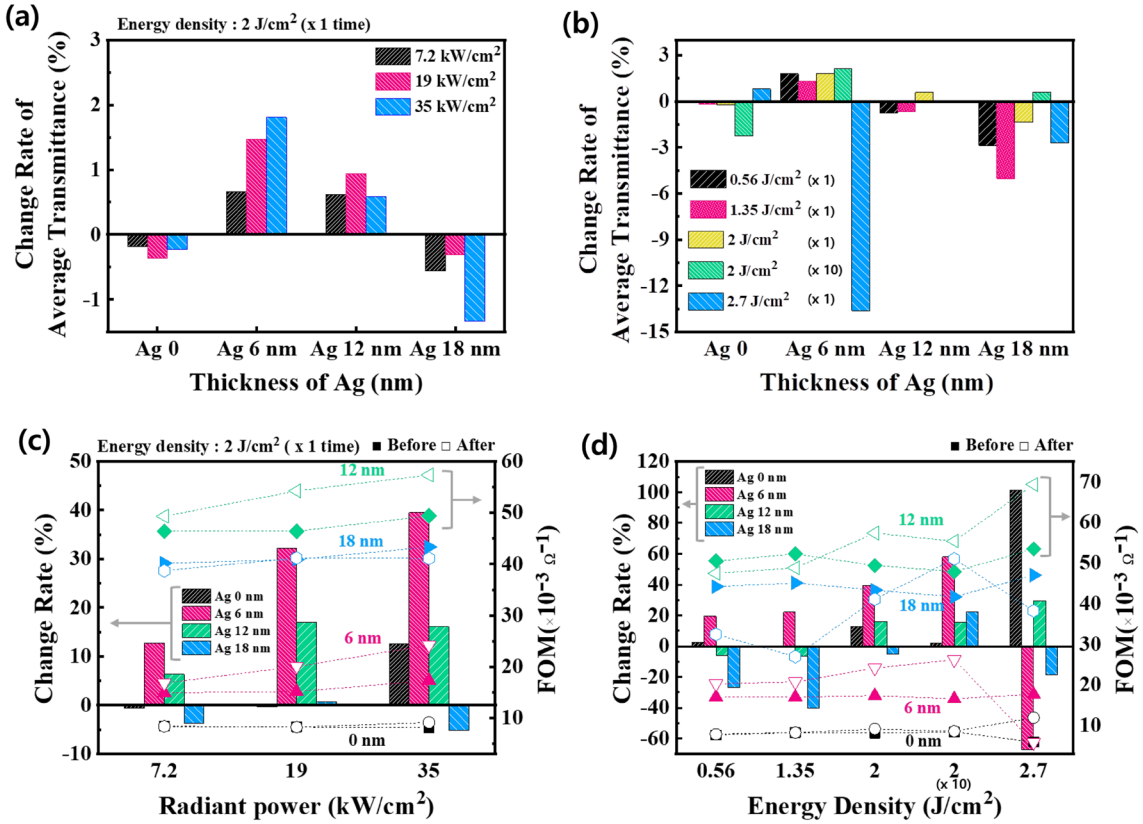

Figure 5. Analysis of optical and FOM properties after Xe-FLA photonic curing: (**a**) Rate of change in average transmittance for different Ag thicknesses and Xe-FLA radiant powers (@ 2 J/cm^2, × 1 time). (**b**) Rate of change in average transmittance for different Ag thicknesses and Xe-FLA radiant energy densities (0.56 J/cm^2–24 kW/cm^2, others–35 kW/cm^2). (**c**) Rate of change in FOM value with respect to Xe-FLA radiant power and Ag thickness (@ 2 J/cm^2, × 1 time). (**d**) Rate of change in FOM value with respect to Xe-FLA energy density and Ag thickness (0.56 J/cm^2–24 kW/cm^2, others–35 kW/cm^2).

Energy density (Repeat)	Ag (nm)	FOM		
		Before Xe-FLA (ohm/sq)	After Xe-FLA (ohm/sq)	Enhancement (%)
2 J/cm^2 (× 1 time)	0	8.12	9.14	12.61
	6	17.34	24.19	39.54
	12	49.41	57.37	16.10
	18	43.32	41.10	− 5.12
2 J/cm^2 (× 10 times)	0	8.42	8.59	2.10
	6	16.59	26.22	58.00
	12	47.85	55.39	15.74
	18	41.69	51.02	22.38

Table 2. Improvement in FOM Value after Applying Xe-FLA photonic curing.

decreased results, because the surface roughness deteriorated slightly (Figs. 5b, 6d). These results indicate that Xe-FLA photonic curing can improve the surface roughness of Ag depending on the conditions, and as a result, the FOM value increased as the transmittance of the multilayer improved.

In this study it was possible to obtain a transparent electrode with a high FOM value by inducing rapid photonic curing effect at high temperature, in the μs time scale, using Xe-FLA, This opens the future possibility of a high-throughput roll-to-roll process, because an extremely low thermal budget was employed. Compared to the transparent ITO–Ag–ITO flexible electrode studied with the previous annealing method, a high FOM value was achieved, even with a very short photonic curing time, as shown in Table 3.

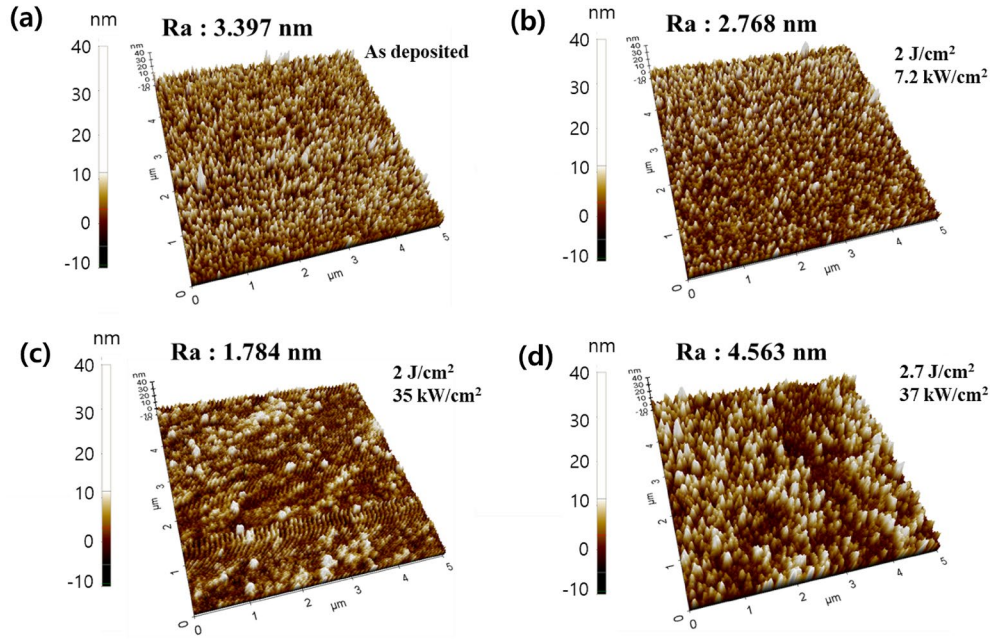

Figure 6. AFM images of ITO (48 nm)-Ag (12 nm)-ITO (48 nm) multilayer, (**a**) as deposited (Ra = 3.397 nm), (**b**) 2 J/cm^2, 7.2 kW/cm^2, 1 repeat (Ra = 2.768 nm), (**c**) 2 J/cm^2, 35 kW/cm^2, 1 repeat (Ra = 1.784 nm), and (**d**) 2.7 J/cm^2, 37 kW/cm^2, 1 repeat (Ra = 4.563 nm).

Structure	FOM (10^{-3}* ohm^{-1})	Resistance (ohm/sq)	Transmittance (%)	Temperature (°C)	Time (sec.)	Thermal budget (Temp. * Time)	Refs.
ITO/Ag/ITO	69.3	6.5	92.3	727	0.0001	0.0727	This work
ITO/Ag/ITO	85.0	6.0	90.0	350	900	315,000	[29]
ITO/Ag/ITO	66.0	10.0	96.0	500	300	150,000	[30]
ITO/Ag/ITO	64.6	6.4	91.4	300	3600	1,080,000	[31]
ITO/Ag/ITO	121.0	3.0	90.2	600	1800	1,080,000	[32]
ITO/Ag/ITO	106.0	3.8	91.3	600	300	180,000	[33]
ITO/Al–Ag/ITO	76.4	2.9	86.1	400	300	120,000	[34]
ITO/Ag/ITO	46.4	6.2	88.2	300	300	90,000	[35]

Table 3. Comparison of annealing conditions and key parameters of ITO–Ag–ITO electrodes.

Conclusion

In summary, we demonstrated a high-quality ITO–Ag–ITO transparent electrode that can be fabricated with high-throughput using Xe-FLA rapid photonic curing, with an extremely low thermal budget. The Xe-FLA annealing temperature was proportional to radiant power, radiant energy, number of irradiations, and the thickness of the Ag, and the thermal budget condition allowed annealing in the range of 100–900 °C for a very short time. When the photonic curing conditions were applied to multilayer ITO–Ag–ITO, the sheet resistance was greatly improved in proportion to the annealing temperature up to about 800 °C. For Ag thicknesses of 6 and 12 nm in the OMO transparent electrode, the highest sheet resistance improvement was observed at annealing conditions (35 kW/cm^2, 2.7 J/cm^2, × 1 time) of about 700 °C.

Since the Ag layer is grown by the Volmer-Weber 3D-island growth model, the Ag layer is not continuously connected at thicknesses below 10 nm, resulting in high sheet resistance. However, after Xe-FLA, SEM images confirmed that a quasi-perfect layer had been formed. Because the Ag thin films were continuously connected, the sheet resistance was greatly improved. In addition, Xe-FLA improved the surface roughness of the ITO–Ag–ITO, and transmittance was also improved. When Xe-FLA was applied, the FOM value of the multilayer electrode with an Ag thickness of 6 nm increased by 58%, and when the Ag thickness was 12 nm, the FOM value reached the maximum value of 69.3.

Materials and methods

ITO–Ag–ITO fabrication. In this experiment, the in-line magnetron sputtering method was used to prepare the OMO multilayer, because magnetron sputtering can deposit thin films uniformly over a large area at a low temperature[51,54]. The OMO multilayer was deposited on a glass substrate (75 × 16 × 1 mm^3) by in-line mag-

netron sputtering. Prior to deposition, the substrate was cleaned with acetone in an ultrasonic cleaner, and then washed with DI water. ITO and Ag layers were deposited using a 540×165 mm^2 ITO target (99.99%) and 4-inch Ag target (99.99%), respectively. The deposition conditions of the ITO and Ag layers are shown in Tables S3 and S4, respectively.

In order to obtain an ITO with high conductivity and stable optoelectrical characteristics, and to prevent excessive oxygen vacancies from being generated, oxygen was appropriately added during the deposition process[55,56]. In order to ensure the uniformity of the deposition, a scanning method was used in the sputtering process. This means that the substrate is moved through the target during the deposition process. The scanning time was set as a variable in the Ag deposition, in order to observe the influence of different thicknesses of Ag layer after annealing the ITO–Ag–ITO multilayer. A high vacuum condition was ensured before sputtering, and the process was carried out at air condition.

Characterization of the OMO electrode. Changes in sheet resistance, transmittance and surface morphology according to the annealing process were observed by 4-point probe, ultraviolet–visible spectroscope (UV–vis) and atomic force microscope (AFM), respectively.

Xe-Flash lamp annealing. PulseForge 1300 (PulseForge Corporation) was used for the flash lamp annealing treatment. As shown in Table S5, four different radiant energies, 0.56, 1.35, 2 and 2.7 J/cm^2, were used in the flash lamp annealing experiment, corresponding to different radiant power and pulse envelopes. Three different radiant powers, 7.2, 19 and 35 kW/cm^2, were adopted under the 2 J/cm^2 condition.

Data availability

The datasets used and/or analyzed during the current study available from the corresponding author on reasonable request.

Received: 8 September 2022; Accepted: 10 January 2023
Published online: 19 January 2023

References

1. Lee, G.-H. *et al.* Multifunctional materials for implantable and wearable photonic healthcare devices. *Nat. Rev. Mater.* **5**, 149–165 (2020).
2. Yun, S. H. & Kwok, S. J. Light in diagnosis, therapy and surgery. *Nat. Biomed. Eng.* **1**, 1–16 (2017).
3. Cima, M. J. Next-generation wearable electronics. *Nat. Biotechnol.* **32**, 642–643 (2014).
4. Jeon, Y. *et al.* Parallel-stacked flexible organic light-emitting diodes for wearable photodynamic therapeutics and color-tunable optoelectronics. *ACS Nano* **14**, 15688–15699 (2020).
5. Jeon, Y. *et al.* Sandwich-structure transferable free-form OLEDs for wearable and disposable skin wound photomedicine. *Light Sci. Appl.* **8**, 1–15 (2019).
6. Wager, J. F. Transparent electronics. *Science* **300**, 1245–1246 (2003).
7. Noh, I. *et al.* Enhanced photodynamic cancer treatment by mitochondria-targeting and brominated near-infrared fluorophores. *Adv. Sci.* **5**, 1700481 (2018).
8. Wang, J. *et al.* A bi-functional device for self-powered electrochromic window and self-rechargeable transparent battery applications. *Nat. Commun.* **5**, 1–7 (2014).
9. Husain, A. A., Hasan, W. Z. W., Shafie, S., Hamidon, M. N. & Pandey, S. S. A review of transparent solar photovoltaic technologies. *Renew. Sustain. Energy Rev.* **94**, 779–791 (2018).
10. Shahzad, F., Iqbal, A., Kim, H. & Koo, C. M. 2D transition metal carbides (MXenes): Applications as an electrically conducting material. *Adv. Mater.* **32**, 2002159 (2020).
11. Lee, K.-T., Park, D. H., Baac, H. W. & Han, S. Graphene-and carbon-nanotube-based transparent electrodes for semitransparent solar cells. *Materials* **11**, 1503 (2018).
12. Ali, A. H., Hassan, Z. & Shuhaimi, A. Enhancement of optical transmittance and electrical resistivity of post-annealed ITO thin films RF sputtered on Si. *Appl. Surf. Sci.* **443**, 544–547 (2018).
13. Kang, D.-W., Kuk, S.-H., Ji, K.-S., Lee, H.-M. & Han, M.-K. Effects of ITO precursor thickness on transparent conductive Al doped ZnO film for solar cell applications. *Sol. Energy Mater. Sol. Cells* **95**, 138–141 (2011).
14. Lee, S. M., Lee, J. M., Kwon, S. J. & Cho, E. S. Effects of post annealing temperatures on sputtered indium tin oxide films for the application to resistive touch panel. *Mol. Cryst. Liq. Cryst.* **586**, 138–146 (2013).
15. Jeong, J.-A. & Kim, H.-K. Low resistance and highly transparent ITO–Ag–ITO multilayer electrode using surface plasmon resonance of Ag layer for bulk-heterojunction organic solar cells. *Sol. Energy Mater. Sol. Cells* **93**, 1801–1809 (2009).
16. Oh, C. S., Lee, H. J., Lee, E. J. & Park, L. S. S. ITO/Ag/ITO multilayer polymer films by roll-to-roll process and performance of flexible OLED devices. *Mol. Cryst. Liq. Cryst.* **551**, 78–85 (2011).
17. Choa, S.-H., Cho, C.-K., Hwang, W.-J., Eun, K. T. & Kim, H.-K. Mechanical integrity of flexible InZnO/Ag/InZnO multilayer electrodes grown by continuous roll-to-roll sputtering. *Sol. Energy Mater. Sol. Cells* **95**, 3442–3449 (2011).
18. Guillen, C. & Herrero, J. TCO/metal/TCO structures for energy and flexible electronics. *Thin Solid Films* **520**, 1–17 (2011).
19. Han, H., Theodore, N. & Alford, T. Improved conductivity and mechanism of carrier transport in zinc oxide with embedded silver layer. *J. Appl. Phys.* **103**, 013708 (2008).
20. Hrostea, L. *et al.* Oxide/metal/oxide electrodes for solar cell applications. *Sol. Energy* **146**, 464–469 (2017).
21. Kang, D. Y. *et al.* Dopant-Tunable ultrathin transparent conductive oxides for efficient energy conversion devices. *Nano Micro Lett.* **13**, 1–15 (2021).
22. Kang, S. K., Kang, D. Y., Park, J. W., Son, K. R. & Kim, T. G. Work function-tunable ZnO/Ag/ZnO film as an effective hole injection electrode prepared via nickel doping for thermally activated delayed fluorescence-based flexible blue organic light-emitting diodes. *Appl. Surf. Sci.* **538**, 148202 (2021).
23. Ko, K.-J. *et al.* Fabrication of an oxide/metal/oxide structured electrode integrated with antireflective film to enhance performance in flexible organic light-emitting diodes. *Mater. Today Energy* **20**, 100704 (2021).
24. Lee, H. J. *et al.* Haze-suppressed transparent electrodes using IZO/Ag/IZO nanomesh for highly flexible and efficient blue organic light-emitting diodes (Advanced Optical Materials 15/2021). *Adv. Opt. Mater.* **9**, 2170055 (2021).
25. Nguyen, V. H. *et al.* Advances in flexible metallic transparent electrodes. *Small* **18**, 2106006 (2022).

26. Lee, J. H., Woo, K. Y., Kim, K. H., Kim, H. D. & Kim, T. G. ITO/Ag/ITO multilayer-based transparent conductive electrodes for ultraviolet light-emitting diodes. *Opt. Lett.* **38**, 5055–5058 (2013).
27. Ahn, M. H., Cho, E. S. & Kwon, S. J. Characteristics of ITO-resistive touch film deposited on a PET substrate by in-line DC magnetron sputtering. *Vacuum* **101**, 221–227 (2014).
28. Song, P. K., Akao, H., Kamei, M., Shigesato, Y. & Yasui, I. Preparation and crystallization of tin-doped and undoped amorphous indium oxide films deposited by sputtering. *Jpn. J. Appl. Phys.* **38**, 5224 (1999).
29. Guillén, C. & Herrero, J. ITO/metal/ITO multilayer structures based on Ag and Cu metal films for high-performance transparent electrodes. *Sol. Energy Mater. Sol. Cells* **92**, 938–941 (2008).
30. Meshram, N., Loka, C., Park, K. R. & Lee, K.-S. Enhanced transmittance of ITO/Ag (Cr)/ITO (IAI) multi-layered thin films by high temperature annealing. *Mater. Lett.* **145**, 120–124 (2015).
31. Wu, C.-C. Highly flexible touch screen panel fabricated with silver-inserted transparent ITO triple-layer structures. *RSC Adv.* **8**, 11862–11870 (2018).
32. Djeffal, F., Ferhati, H., Benhaya, A. & Bendjerad, A. Effects of high temperature annealing in enhancing the optoelectronic performance of sputtered ITO/Ag/ITO transparent electrodes. *Superlattices Microstruct.* **130**, 361–368 (2019).
33. Lee, S. Y., Park, Y. S. & Seong, T.-Y. Optimized ITO/Ag/ITO multilayers as a current spreading layer to enhance the light output of ultraviolet light-emitting diodes. *J. Alloy. Compd.* **776**, 960–964 (2019).
34. Isiyaku, A. K., Ali, A. H. & Nayan, N. Structural optical and electrical properties of a transparent conductive ITO/Al–Ag/ITO multilayer contact. *Beilstein J. Nanotechnol.* **11**, 695–702 (2020).
35. Jeong, J.-A., Kim, H.-K., Koo, H.-W. & Kim, T.-W. Transmission electron microscopy study of degradation in transparent indium tin oxide/Ag/indium tin oxide multilayer films. *Appl. Phys. Lett.* **103**, 011902 (2013).
36. Choi, K., Kim, J., Lee, Y. & Kim, H. ITO/Ag/ITO multilayer films for the application of a very low resistance transparent electrode. *Thin Solid Films* **341**, 152–155 (1999).
37. Schroder, K., Rawson, I. M., Pope, D. S. & Farnsworth, S. in *International Symposium on Microelectronics* 001040–001046 (International Microelectronics Assembly and Packaging Society).
38. Daunis, T. B., Schroder, K. A. & Hsu, J. W. Photonic curing of solution-deposited ZrO2 dielectric on PEN: a path towards high-throughput processing of oxide electronics. *npj Flex. Electron.* **4**, 1–7 (2020).
39. Kim, Y., Park, S., Kim, B.-K., Kim, H. J. & Hwang, J.-H. Xe-arc flash annealing of indium tin oxide thin-films prepared on glass backplanes. *Int. J. Heat Mass Transf.* **91**, 543–551 (2015).
40. Hwang, J.-H. *et al.* Scanning multishot irradiations on a large-area glass substrate for Xe-Arc flash lamp crystallization of amorphous silicon thin-film. *Int. J. Therm. Sci.* **91**, 1–11 (2015).
41. Das, S. *et al.* Low thermal budget, photonic-cured compact TiO_2 layers for high-efficiency perovskite solar cells. *J. Mater. Chem. A* **4**, 9685–9690 (2016).
42. Plumley, J. B. *et al.* Crystallization of electrically conductive visibly transparent ITO thin films by wavelength-range-specific pulsed Xe arc lamp annealing. *J. Mater. Sci.* **53**, 12949–12960 (2018).
43. Shrestha, M., Wang, K., Zheng, B., Mokrzycki, L. & Fan, Q. H. Comparative study of furnace and flash lamp annealed silicon thin films grown by plasma enhanced chemical vapor deposition. *Coatings* **8**, 97 (2018).
44. Schroder, K., McCool, S. & Furlan, W. Broadcast photonic curing of metallic nanoparticle films. *NSTI Nanotech May* **7**, 11 (2006).
45. Almadhoun, M. N. *et al.* UV-induced ferroelectric phase transformation in PVDF thin films. *Adv. Electron. Mater.* **5**, 1800363 (2019).
46. Kim, R. H. *et al.* Photonic crystallization of two-dimensional MoS_2 for stretchable photodetectors. *Nanoscale* **11**, 13260–13268 (2019).
47. Schroder, K. A. Mechanisms of photonic curing: Processing high temperature films on low temperature substrates. *Nanotechnology* **2**, 220–223 (2011).
48. Kneipp, K., Kneipp, H., Itzkan, I., Dasari, R. R. & Feld, M. S. Surface-enhanced Raman scattering and biophysics. *J. Phys. Condens. Matter* **14**, R597 (2002).
49. Gulen, M. *et al.* Role of annealing temperature on microstructural and electro-optical properties of ITO films produced by sputtering. *J. Mater. Sci. Mater. Electron.* **24**, 467–474 (2013).
50. Sui, M. *et al.* Evolution of self-assembled Ag nanostructures on c-plane sapphire by the systematic control of annealing temperature. *Superlattices Microstruct.* **100**, 1128–1142 (2016).
51. Lee, S. Y., Cho, E.-S. & Kwon, S. J. The optical analyses of the multilayer transparent electrode and the formation of ITO/Mesh-Ag/ITO multilayers for enhancing an optical transmittance. *Appl. Surf. Sci.* **487**, 990–999 (2019).
52. Kim, D. Y., Han, Y. C., Kim, H. C., Jeong, E. G. & Choi, K. C. Highly transparent and flexible organic light-emitting diodes with structure optimized for anode/cathode multilayer electrodes. *Adv. Funct. Mater.* **25**, 7145–7153 (2015).
53. Park, S.-H. *et al.* Large area roll-to-roll sputtering of transparent ITO/Ag/ITO cathodes for flexible inverted organic solar cell modules. *Org. Electron.* **30**, 112–121 (2016).
54. Takeda, S., Suzuki, S., Odaka, H. & Hosono, H. Photocatalytic TiO_2 thin film deposited onto glass by DC magnetron sputtering. *Thin Solid Films* **392**, 338–344 (2001).
55. Cho, S. *et al.* Effects of O_2 addition on microstructure and electrical property for ITO films deposited with several kinds of ITO targets. *J. Phys. Chem. Solids* **69**, 1334–1337 (2008).
56. Kim, Y.-S. *et al.* Influence of O_2 admixture and sputtering pressure on the properties of ITO thin films deposited on PET substrate using RF reactive magnetron sputtering. *Surf. Coat. Technol.* **173**, 299–308 (2003).

Acknowledgements

The Xe-FLA process was operated with the help of Hanseul Kim, Minyoung Lee, and Jaerin Kim from the Pulse Forge Corporation**.** This research was supported by a grant of the Korea Health Technology R&D Project through the Korea Health Industry Development Institute (KHIDI), funded by the Ministry of Health & Welfare, Republic of Korea (Grant Number: HI22C0290). Also, this research was also funded by the Gachon University research fund of 2019 (GCU–2019–0764).

Author contributions

Y.J. and E.-S.C. designed the idea for rapid photonic curing of transparent electrodes using Xe-FLA. Z.Z. conducted experiments and optimizations for ITO–Ag–ITO fabrication and photonic curing in this study. A.R. performed annealing temperature simulation and optimization according to the Xe-FLA condition. S.J.K. performed transmittance simulation for the transparent electrode in this study. All authors discussed the experiment and participated in preparing the paper. Y.J and E.-S.C. contributed equally as the corresponding author.

Competing interests

The authors declare no competing interests.

Additional information

Supplementary Information The online version contains supplementary material available at https://doi.org/10.1038/s41598-023-27942-4.

Correspondence and requests for materials should be addressed to Y.J. or E.-S.C.

Reprints and permissions information is available at www.nature.com/reprints.

Publisher's note Springer Nature remains neutral with regard to jurisdictional claims in published maps and institutional affiliations.